Cell

Control of the Mitotic Cleavage Plane by Local Epithelial Topology

William T. Gibson,[1,2,3,5] James H. Veldhuis,[4] Boris Rubinstein,[3] Heather N. Cartwright,[3] Norbert Perrimon,[5] G. Wayne Brodland,[4] Radhika Nagpal,[2] and Matthew C. Gibson[3,6,*]
[1]Program in Biophysics
[2]School of Engineering & Applied Sciences
Harvard University, Cambridge, MA 02138, USA
[3]Stowers Institute for Medical Research, Kansas City, MO 64110, USA
[4]Department of Civil and Environmental Engineering, University of Waterloo, Waterloo, ON N2L 3G1, Canada
[5]Department of Genetics, Howard Hughes Medical Institute, Harvard Medical School, Boston, MA 02115, USA
[6]Department of Anatomy and Cell Biology, Kansas University Medical Center, Kansas City, KS 64110, USA
*Correspondence: mg2@stowers.org
DOI 10.1016/j.cell.2010.12.035

SUMMARY

For nearly 150 years, it has been recognized that cell shape strongly influences the orientation of the mitotic cleavage plane (e.g., Hofmeister, 1863). However, we still understand little about the complex interplay between cell shape and cleavage-plane orientation in epithelia, where polygonal cell geometries emerge from multiple factors, including cell packing, cell growth, and cell division itself. Here, using mechanical simulations, we show that the polygonal shapes of individual cells can systematically bias the long-axis orientations of their adjacent mitotic neighbors. Strikingly, analyses of both animal epithelia and plant epidermis confirm a robust and nearly identical correlation between local cell topology and cleavage-plane orientation in vivo. Using simple mathematics, we show that this effect derives from fundamental packing constraints. Our results suggest that local epithelial topology is a key determinant of cleavage-plane orientation, and that cleavage-plane bias may be a widespread property of polygonal cell sheets in plants and animals.

INTRODUCTION

The active control of the mitotic cleavage plane is crucial to numerous processes, and the consequences of cleavage-plane misorientation can be catastrophic, ranging from polycystic kidney disease and organ malformation to tumorigenesis (Baena-López et al., 2005; Fischer et al., 2006; Gong et al., 2004; Quyn et al., 2010; Saburi et al., 2008). Although the control of cleavage-plane orientation is usually understood from a molecular viewpoint (Buschmann et al., 2006; Fernández-Miñán et al., 2007; Johnston et al., 2009; Siller and Doe, 2009; Speicher et al., 2008; Théry et al., 2005; Traas et al., 1995; Vanstraelen et al., 2006; Walker et al., 2007; Wright et al., 2009), more than a century of observations show that mitotic cells in both plants and animals tend to divide orthogonal to their geometric long axis as a default mechanism (Gray et al., 2004; Hofmeister, 1863; O'Connell and Wang, 2000; Strauss et al., 2006). In plants, the geometric location of the division plane can be predicted by cytoskeletal structures (Kost and Chua, 2002; Palevitz, 1987; Pickett-Heaps and Northcote, 1966; Sinnott and Bloch, 1940), and biophysical experiments suggest that the cytoskeleton may be involved in the process of orienting the division plane as dictated by cell geometry (Flanders et al., 1990; Goodbody et al., 1991; Katsuta et al., 1990; Lloyd, 1991). Further, in animal cells, recent studies implicate the geometry of cell-matrix adhesions as a key determinant of cleavage-plane orientation (Théry et al., 2005, 2007). Cell geometry is thus a critical determinant of cleavage-plane orientation, at both the molecular and biophysical levels.

Whereas the regulation of mitotic cleavage-plane orientation by geometric cues has been extensively probed in unicellular systems, far less attention has been given to adherent epithelial and epidermal layers. In this context, cell geometry does not exist in isolation because cell shapes emerge from the combined effects of growth, mitosis, and cellular packing. A priori, this complex interplay of biological processes, and the diverse genetic programs that have evolved to control them in plants and animals, would appear to suggest a staggering range of possible cell geometries within an epithelium. However, spatial considerations impose powerful constraints on the shapes of cells in monolayer sheets, from the distribution of polygonal cell types (Rivier et al., 1995) to their neighbor correlations (Peshkin et al., 1991) and relative sizes (Rivier and Lissowski, 1982). Indeed, empirical investigation confirms that many monolayer cell sheets across the plant and animal kingdoms converge on a default equilibrium distribution of cellular shapes, with approximately 45% hexagons, 25% pentagons, and 20% heptagons (Gibson et al., 2006; Korn and Spalding, 1973; Lewis, 1928). Such clear conservation of cellular network architecture raises the question as to whether conserved cellular division mechanisms are responsible for generating such similar packing arrangements of cells, as numerous studies have proposed (Dubertret et al., 1998; Gibson et al., 2006; Korn and Spalding, 1973; Miri and Rivier, 2006; Patel et al., 2009). The strongest

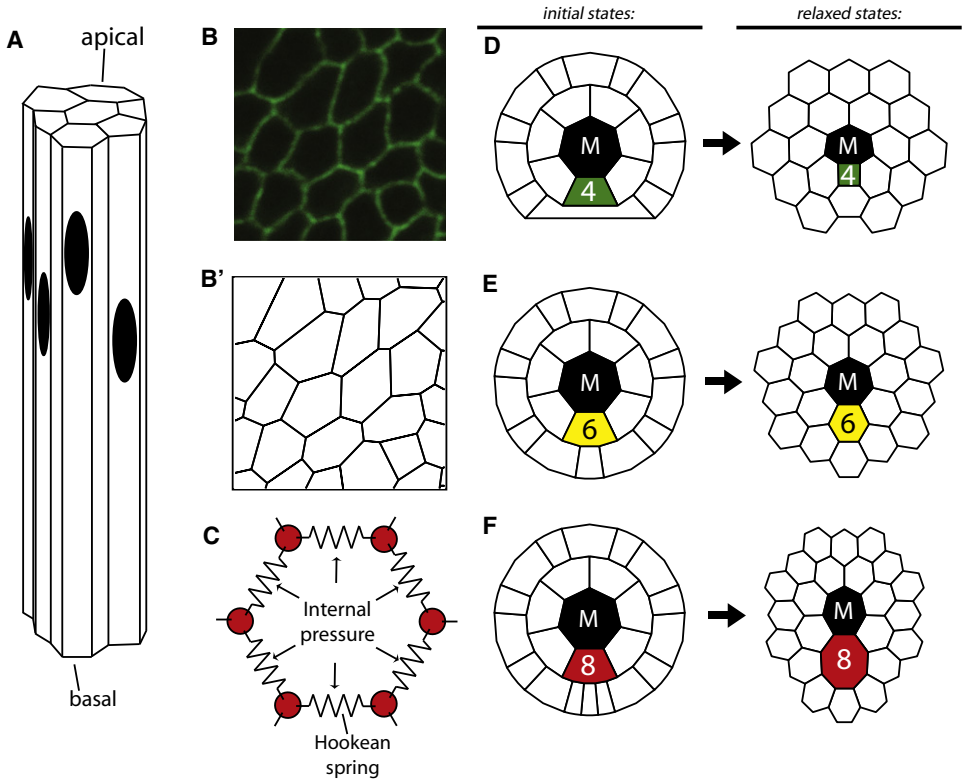

Figure 1. Local Epithelial Topology Is Predicted to Influence the Geometry of an Epithelial Cell

(A) A stereotypical simple columnar epithelium. Black spots represent nuclei.

(B) The *Drosophila* wing disc epithelium, with NRG-GFP (green) marking the septate junctions.

(B′) A planar network representation of (B).

(C) A model for finding the minimum energy configuration of cell packing, based on internal pressure and ideal springs.

(D–F) (Initial states, left) Initial conditions for the relaxation algorithm. Each case varies the topology of the marked cell. (Relaxed states, right) At equilibrium, cell shape is specified by a balance between pressure and tension. The central cell's shape is strongly influenced by the labeled cell's topology.

See also Figure S1.

evidence to date that common mechanisms are used among plants and animals to generate conserved packing relationships can be found in the *mitotic shift*, wherein the distribution of mitotic cell shapes is shifted by a single polygon class to have a heptagonal mean, as opposed to a hexagonal mean as seen in interphase cells.

Here, we use computational modeling, experimental observation, and mathematical analysis to report that, as a default property, neighbor cell shape can strongly bias cleavage-plane orientation in the monolayer cell sheets of both plants and animals. Intriguingly, we show that this bias increases the structural regularity of an epithelium by increasing the frequency of hexagons. Our analysis indicates that simultaneously, cleavage-plane bias is also involved in specifying the mitotic shift. The mechanism through which cleavage-plane bias accomplishes these effects is differential side-gaining, whereby dividing cells preferentially cleave their common interfaces with subhexagonal cells such as quadrilaterals and avoid cleaving their common interfaces with superhexagonal cells such as octagons. Together, our results suggest a common emergent mechanism in plants and animals for the control of tissue-level architecture by packing-mediated control of the mitotic cleavage plane.

RESULTS

The Shape of a Cell Is Predicted to Be Influenced by Local Topology

In epithelia, the tissue-level architecture at the apical junctions is a contiguous tiling of polygonal cell shapes (Figures 1A and 1B). This pattern can be described as a simple planar network wherein a cell's number of neighbors (topology) is equivalent to its polygon class (Figure 1B′). To investigate the effect of polygonal cell packing on mitotic cell shape, and by extension, cleavage-plane orientation, we tested whether a cell's long axis is systematically influenced by the polygon class of neighboring cells.

To address this, we numerically solved for the minimal energy configuration of a local cellular neighborhood (Prusinkiewicz and Lindenmayer, 1990), defined to be a central mitotic cell (*M*) and its first-order polygonal neighbors. Geometrically, cells were idealized as polygonal prisms with constant height (Figure 1A).

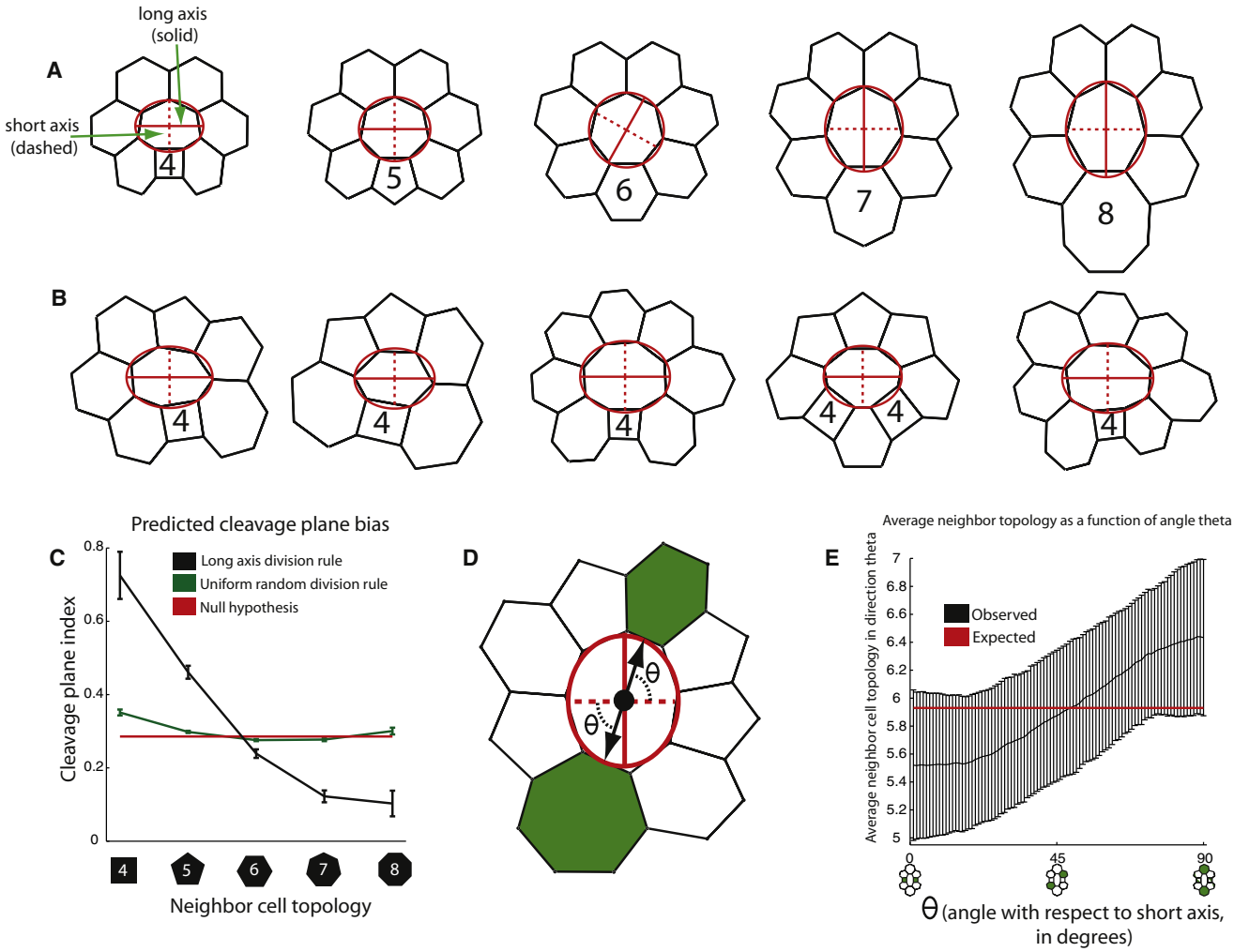

Figure 2. The Orientation of a Cell's Short Axis Is Predicted to Correlate with Its Quadrilateral and Pentagonal Neighbors and to Anticorrelate with Heptagonal and Octagonal Neighbors

(A) Neighbor cell topology, N, influences the direction of the cellular long axis (solid line) and short axis (dashed line), based on an ellipse of best-fit (red). Second-order and higher neighbors, which are uniformly hexagonal, are not shown. For $N < 6$, the short axis is oriented toward the N-sided cell *N*; for $N > 6$, it is oriented perpendicular to *N*.

(B) The attraction of the short axis to quadrilateral cells ($N = 4$) is robust to heterogeneity in the local cell neighborhood.

(C) We computed the cleavage-plane index, or fraction of neighbors in each polygon class (black line) located adjacent to the central cell's short axis (presumed cleavage plane). Neighbor cells having $N < 6$ are significantly enriched in this position. Conversely, neighbors having $N > 6$ are underrepresented. For comparison, for a randomly oriented division plane, all N values occur with similar frequency (green), which is close to the null hypothesis of 2/7 (red). Error bars represent ±1 standard deviation (SD).

(D) We defined an acute angle, θ, with respect to a cell's short axis (dashed red line), as well as the neighbor topology in direction θ (green cells).

(E) On average, neighbor topology (black) is an increasing function of acute angle θ. Error bars represent the standard deviation in the sample mean topology in direction θ per cell (an average of the four positions on the cell cortex corresponding to the θ, over 420 such cells).

For relaxation, cell mechanics were modeled in terms of a balance between edge-length tensions, described using ideal springs, and internal pressure, modeled as an ideal gas (Figure 1C). The central mitotic cell, *M*, was a heptagon, consistent with the fact that the average mitotic cell is seven-sided in vivo (Aegerter-Wilmsen et al., 2010; Gibson et al., 2006). Parameters were chosen to be uniform for every cell, and initial conditions were arbitrary (Figures 1D–1F). Given these choices, the effect of local topology on the shape of the central cell was an emergent property of the relaxed mechanical network at equilibrium (Figures 1D–1F; Figure S1 available online; Extended Experimental Procedures).

To analyze the impact of local topology on the long axis of *M*, we replaced one neighbor hexagon with a single N-sided cell, *N*. Strikingly, inserting any nonhexagonal neighbor induced a clear long axis in *M*, with opposite orientation of the long axis for $N < 6$ versus $N > 6$ (Figures 1D–1F; Figure 2A). Specifically, the presence of quadrilateral or pentagonal neighbors induced a long

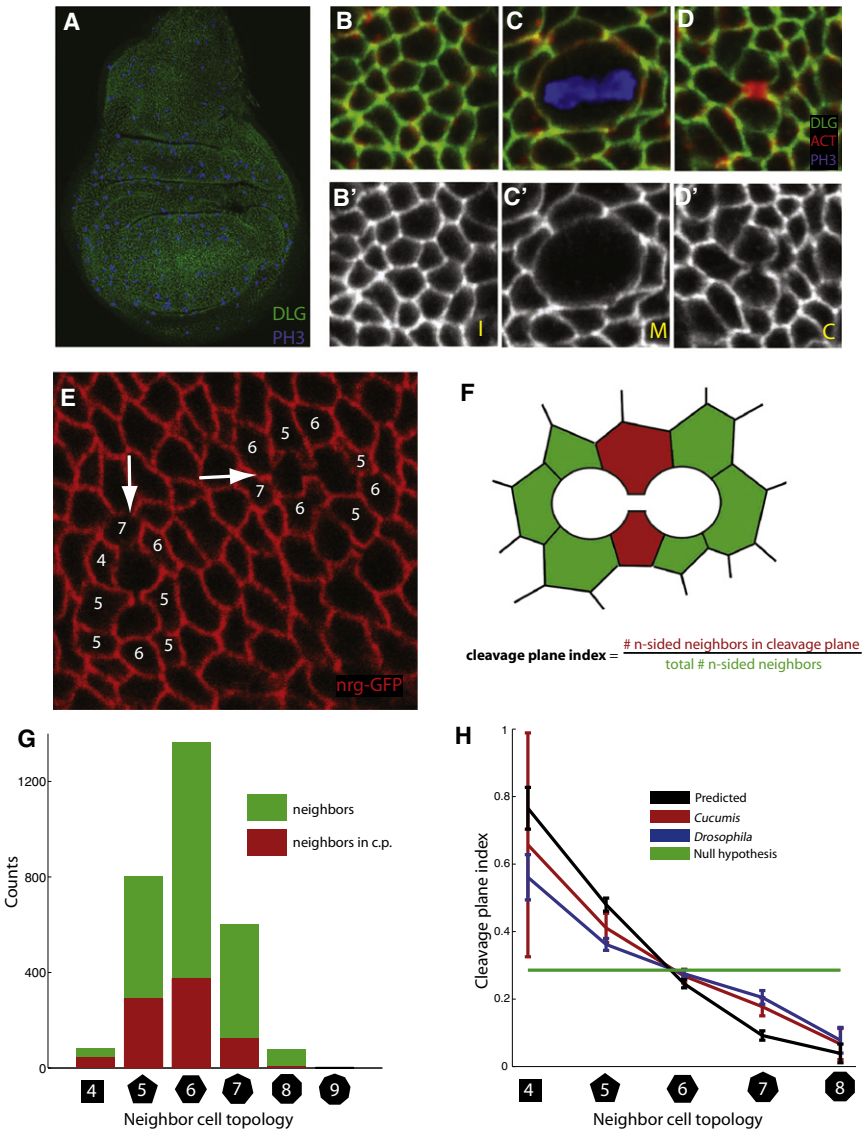

Figure 3. In Both Plants and Animals, a Dividing Cell's Cleavage Plane Correlates with Its Quadrilateral and Pentagonal Neighbors and Anticorrelates with Heptagonal and Octagonal Neighbors

(A) The *Drosophila* wing imaginal disc, stained with anti-DLG to mark the junctions (green) and anti-PH3 to mark chromatin (blue).

(B–D and B′–D′) Cell division proceeds in the plane of the epithelium via a stereotyped division process including interphase (I), mitosis (M), and cytokinesis (C). Actin staining is shown in red.

(E) We can infer the topological complement of neighbors, as well as the division orientation of dividing cells, from cytokinetic figures. Junctions are marked by an *nrg-gfp* protein trap (red).

(F and G) We examined >400 such figures and sorted the neighbors by polygon class. The neighbors on the division plane (red) are a subset of the full complement of neighbors (green and red).

(H) An overlay of the predicted mitotic cleavage-plane bias based on our mechanical model (black), with the biases computed from both *Drosophila* wing disc epithelium (blue) and cucumber epidermis (red). Each is compared with the topological null hypothesis (green). Note that here the mechanical model (black) uses the empirically derived local neighborhood topologies for direct comparison with the *Drosophila* data (blue). Error bars represent ±1 SD.

See also Figure S2 for further information.

axis parallel to the *NM* interface, whereas heptagons and octagons induced a long axis orthogonal to interface *NM*. These results suggest that in cell sheets, the orientation of a mitotic cell's longest axis can be strongly influenced by the polygon class of a single neighboring cell. As a consequence of this effect, neighbor cells with fewer sides (such as quadrilaterals and pentagons) tend to lie along the shortest axis of M, which is the location of the presumed cleavage plane.

To test whether this effect was robust under more realistic conditions, we numerically relaxed heterogeneous local neighborhoods that were stochastically generated from the known polygonal cell shape distribution of the *Drosophila melanogaster* wing epithelium (Figure 2B) (Aegerter-Wilmsen et al., 2010; Gibson et al., 2006). Even under these conditions, more than 70% of quadrilateral neighbors were positioned on the central cell's short axis, double the percentage expected by chance (Figure 2C). To quantify this relationship, we defined an acute angle, θ, with respect to the presumed cleavage plane along the central cell's short axis (see Figure 2D). On average, as a function of increasing θ, the neighbor polygon class in direction θ increased monotonically (Figure 2E). Therefore, even in a heterogeneous context, the topology of a cellular neighborhood robustly and systematically influenced the orientation of the long axis in a central cell.

Cleavage-Plane Bias in the *Drosophila* Wing Disc

In both plants and animals, cells are thought to divide their long axis by forming a cleavage plane along the short axis of the cell (Hofmeister, 1863; Strauss et al., 2006). If a cell's short axis consistently bisects its cellular neighbors having the fewest sides (Figure 2), then mitotic division planes should be disproportionately biased toward quadrilaterals and pentagons in vivo. To test this, we measured the correlation between neighbor cell polygon class and cleavage-plane orientation in the *Drosophila* wing imaginal disc (Figure 3A). Here, cell division proceeds through a stereotyped process of cell rounding at the apical epithelial surface (Figures 3B–3D) (Gibson et al., 2006). To define the frequency with which different classes of polygonal

neighbors were bisected by the cleavage plane, we examined 420 cells at the cytokinetic stage, which is the most stable and easily scored phase of mitosis (Figure 3E). For each case, we recorded the position of all primary neighboring polygons and computed the frequency with which each polygon class occupied the cleavage-plane position (Figures 3F and 3G).

If the orientation of cell division were random with respect to local topology, approximately 28.6% of any given polygon class would be expected to correlate with the cleavage plane (two randomly chosen cells out of seven neighbors). However, in the wing disc, we found that more than 50% of quadrilaterals in the primary neighborhood occupied the division plane position (Figure 3H; n = 46/83). Further, octagons were anticorrelated with the division plane and occupied that position with less than 10% probability (n = 6/77). As predicted by the mechanical model, this cleavage-plane bias was monotone decreasing across all polygon types. We conclude that in the *Drosophila* wing disc, the polygonal topology of local neighborhoods strongly influences cleavage-plane orientation in mitotic cells.

In order to test the assumption that *Drosophila* wing disc cells actually divide their longest axis, we next performed time-lapse analysis of proliferating *Drosophila* wing discs in ex vivo culture (see Movie S1; Experimental Procedures). For each of 198 mitotic cells (Figure 4A), we measured the geometric long-axis orientation during both interphase (Figure 4A′, far left) and cytokinesis (Figure 4A′, far right). We found a strong tendency for cells to follow a long-axis division mechanism, although with moderate noise in the orientation (Figure 4B). This tendency to divide the longest axis correlated with the interphase geometry (Figure 4B) and increased with the cell's interphase elongation ratio (the ratio of the long axis to the short axis; Extended Experimental Procedures). For example, for the 99 cells having an elongation ratio below the median value of 1.68, the average deviation from a long-axis division mechanism was about 33°; by contrast, for the 99 cells having an elongation ratio above the median value, the average deviation was about 21° (data not shown). This dependence on the relative axis lengths suggests that these cells might be able to adjust their spindle orientations to their newly acquired shapes following mechanical strain, as has been previously reported in cell culture and in vertebrate embryonic cells (Black and Vincent, 1988; Gray et al., 2004; O'Connell and Wang, 2000; Strauss et al., 2006).

To test whether deviation from the long-axis division mechanism could explain the discrepancy between our cleavage-plane bias predictions and the empirical measurements, we incorporated the measured deviation into our original model (Figure 4C; Extended Experimental Procedures). Interestingly, when the measured deviation was incorporated, the mechanical predictions were significantly improved (compare the red and black curves in Figure 4C), closely matching the empirically measured bias (Figure 4C, blue curve). Therefore, cleavage-plane bias is likely to be robust to noise in the cleavage-plane mechanism and may be present even when cell divisions do not perfectly obey a long-axis division scheme.

Cleavage-Plane Bias in Plant Epidermis

Because our original predictions were mechanically motivated (Figure 1 and Figure 2), and are expected to persist even when there is moderate noise in the cleavage plane (Figure 4), we reasoned that cleavage-plane bias should be equally likely to appear in plant tissues. To test this, we used data from F.T. Lewis's classical study of cucumber epidermal cell topology (*Cucumis sativus*) to compute the probability with which an N-sided polygonal cell occupies the division plane of a mitotic neighbor (Extended Experimental Procedures) (Lewis, 1928). Remarkably, in *Cucumis*, the cleavage-plane bias was almost indistinguishable from that measured in the *Drosophila* wing disc (Figure 3H). We once again observed strong enrichment for 4-sided cells along the cleavage planes of mitotic cells, whereas 8-sided cells were underrepresented. In order to verify our inferences from Lewis's data (1928), we also directly examined the relationship between local topology and cellular long-axis orientation in the epidermis of *Cucumis* (Figure S3A). From fixed samples of cucumber epidermis, we studied a population of 501 epidermal cells having the same polygonal distribution as the original population of 500 mitotic cells studied by Lewis (1928). Cells were selected in a spatially constrained, impartial manner based solely on polygon class (Extended Experimental Procedures). We next tested whether a naive long-axis division rule was sufficient to generate cleavage-plane bias in *Cucumis*. Based on an ellipse of best fit to each cell's geometry (Figure S3A; Extended Experimental Procedures), we were able to reproduce not only the cleavage-plane enrichment observed in Lewis's original data (Figure S3C) but also the inferred cleavage-plane bias (Figure S3D). Taken together, our results suggest that cleavage-plane bias occurs in polygonal cell sheets as an emergent effect of cell packing, independent of species-specific considerations.

Cleavage-Plane Bias and the Topological Constraints on Cell Geometry

The quantitative similarity of cleavage-plane bias in plants, animals, and in silico suggests that the underlying mechanism is geometric, rather than molecular. In fact, fundamental geometric constraints imposed by the internal angles of neighboring polygons are sufficient to explain this phenomenon. For illustration, consider the comparison between a tiling of three hexagons versus two hexagons and a square (Figures 5A and 5B). From elementary geometry, a square (N = 4) has internal angles of 90°, whereas the internal angles of a hexagon (N = 6) average 120° (for an N-sided polygon, average internal angles are $180°(N-2)/N$). In the context of a contiguous layer, the presence of 90° internal angles within the square forces the internal angles of the adjacent hexagon to increase to 135° (Figure 5B). Intuitively, this deformation results in elongation of these hexagons parallel to the interface with the square, thus generating a cellular long axis.

The constraints imposed by the internal angles of one cell upon the long axis of its neighbor can be formalized for the arbitrary case of an N-sided cell, surrounded by N symmetric hexagonal neighbors (Figure 5C). Assume that a mitotic cell, M, is situated vertically above cell N, resulting in a horizontal interface NM of length L. In the simplest case, all side lengths, including L, are equal and without loss of generality can be set to one. Further, the internal angles α_N and β_M can be

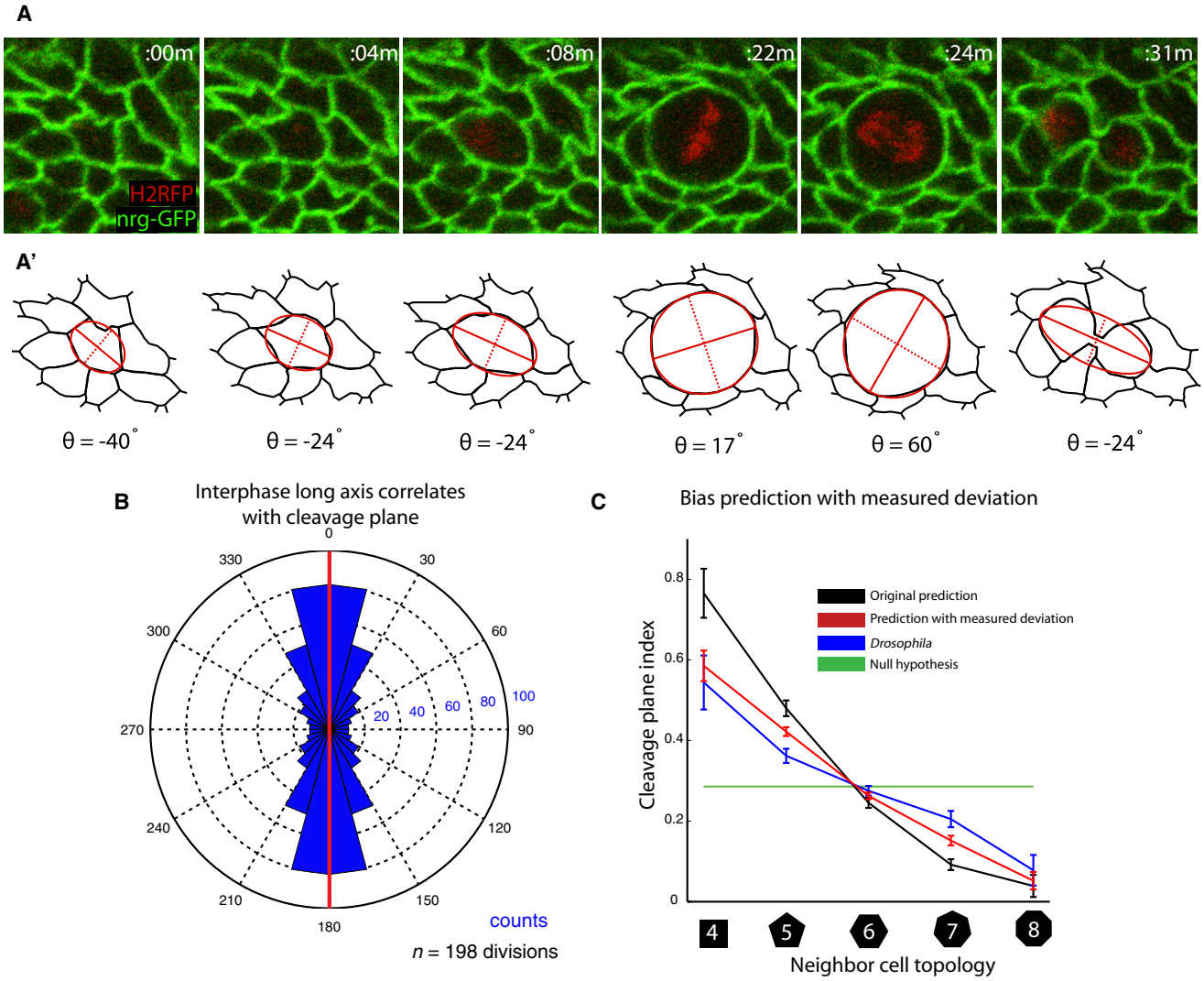

Figure 4. *Drosophila* Wing Disc Cells Approximately Obey a Long-Axis Division Rule

(A) Time series analysis illustrates the process in which an interphase cell entering mitosis gradually dilates before reaching full rounding, and then subsequently undergoes cytokinesis, in an orientation approximately predicted by its interphase long axis.

(A′) Drawings of the process described in the corresponding panels in (A), including the mitotic cell and its immediate neighbors. The long axis of the ellipse of best fit (red) is labeled with a solid line, whereas the dashed line (predicted cleavage plane) represents the short axis.

(B) The eventual orientation of the cleavage plane can be predicted based on the interphase long-axis orientation. The red line (zero deviation from long-axis division) represents a perfect correlation between the interphase long axis and the long axis of the resulting cytokinetic figure. Blue bars show the number of cells (represented by radial distance from the center) that divided with a particular angular deviation from the interphase long axis. On average, the deviation was approximately 27.1 degrees. The data are represented by the first quadrant (0° to 90°), which is also displayed symmetrically in the other three quadrants (90° to 360°).

(C) The bias curve prediction that incorporates the measured deviation of 27° from the long axis (red) is significantly closer to the empirically measured cleavage-plane bias (blue) than the naive long-axis prediction is (black). A Gaussian noise model with 27° standard deviation gives a similar result (data not shown). We controlled for the influence of topological relationships by using the same local neighborhoods as were measured from the empirical data (blue).

Error bars represent ±1 SD. See also the Extended Experimental Procedures and Figure S3, which suggests that a long-axis mechanism may also operate in *Cucumis*.

computed as a function of N. Using simple trigonometry and exploiting the symmetric configuration of neighbors, we can solve for the ratio of the horizontal axis, d_m, to the vertical axis, h_m, for the ellipse of best fit to cell M (Figure 5C; Extended Experimental Procedures):

$$\frac{d_m}{h_m} \approx \sec\left(\frac{\pi}{N}\right)\sqrt{\sin\left(\frac{\pi}{N}\right)\left(1+\sin\left(\frac{\pi}{N}\right)\right)} \quad (1)$$

In this framework, the direction of M's short axis (presumed cleavage plane) is described by the ratio d_m:h_m, which the above

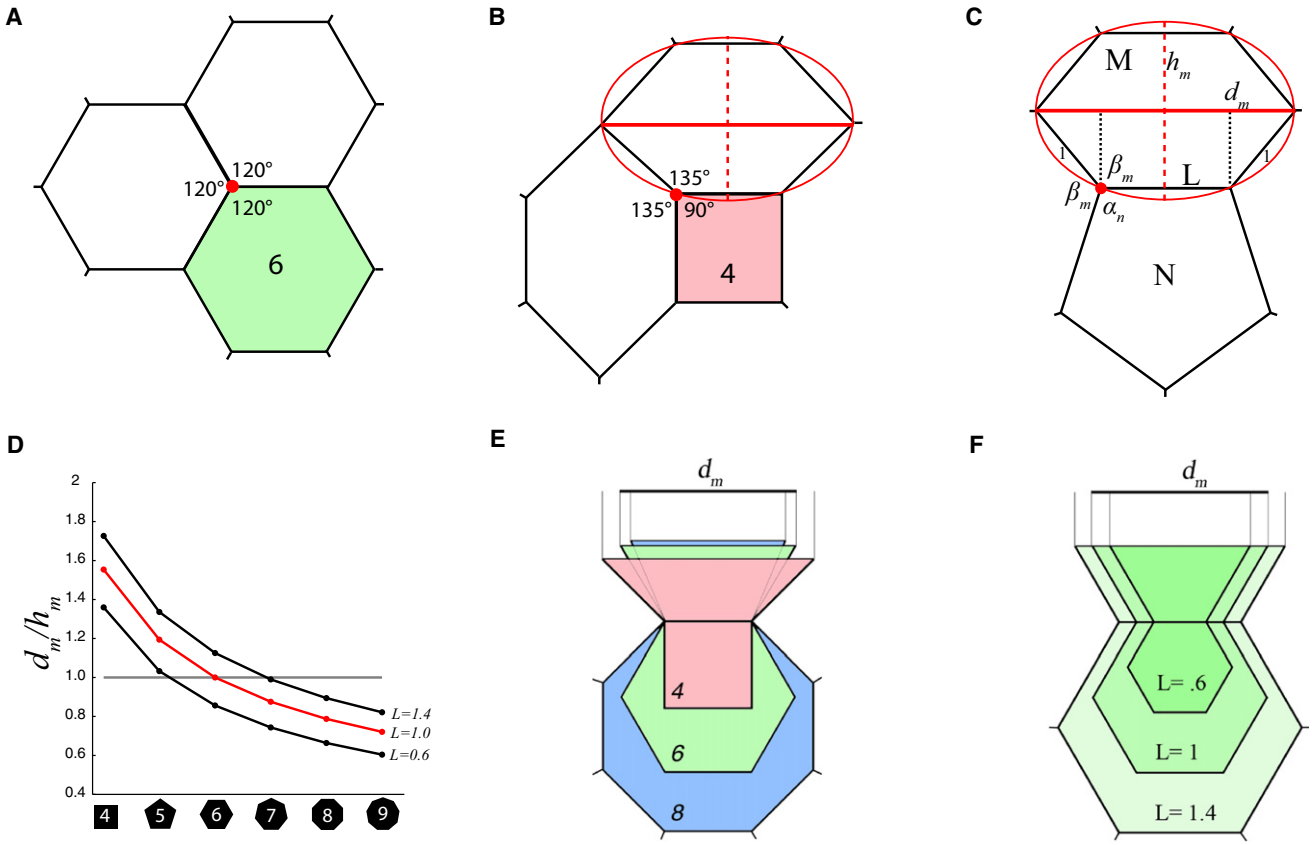

Figure 5. Fundamental Packing Constraints Are Sufficient to Explain Cleavage-Plane Bias

(A) Hexagons pack at 120° angles.

(B) A four-sided cell distorts the internal angles of the surrounding hexagons, inducing a long axis.

(C) A geometrical argument for division-plane bias. The N-sided neighbor cell influences the ratio of the horizontal axis, d_m, to the vertical axis, h_m, in the *M*-cell. When d_m:h_m > 1, the N-cell is in the predicted cleavage-plane position for the *M*-cell.

(D) A plot of the ratio d_m:h_m for different values of N and L. Above the gray line, the N-cell is in the *M*-cell's predicted division plane; the opposite is true below the gray line.

(E and F) Both N and L influence the direction of the long axis in the *M*-cell. (E) The value of N influences the direction of the long axis in the *M*-cell (top cell) for constant L. (F) The long axis of the *M*-cell is influenced by the side length, L, for a constant N value.

See also Figure S4.

equation shows is determined by the N value (Figure 5D). Geometrically, the ratio d_m:h_m varies with N because the length d_m decreases for N > 6 and increases for N < 6 (Figure 5E). Consequently, when N > 6 (d_m:h_m < 1), d_m forms the short axis parallel to interface *NM*. Conversely, if N < 6 (d_m:h_m > 1), then h_m forms the short axis, or presumed cleavage plane, in the direction of *N*, perpendicular to the interface *NM*.

Cleavage-Plane Bias Is Predicted to Be Robust to Side Length and Cell Size Differences

Intuitively, differential side lengths of N-sided neighbors would also affect the short-axis orientation of *M* (Figure 5F). To analyze the relative contributions of angular constraints versus side lengths, consider the more realistic case when the edge lengths are nonuniform (L≠1). Here, d_m:h_m depends on both N and L (Figure 5D and Extended Experimental Procedures):

$$\frac{d_m}{h_m} \approx \sec\left(\frac{\pi}{N}\right)\sqrt{\sin\left(\frac{\pi}{N}\right)\left(L+\sin\left(\frac{\pi}{N}\right)\right)} \qquad (2)$$

For the simplified case when L = 1, the direction of the short axis undergoes a 90° rotation (between horizontal and vertical) when d_m:h_m passes through the value 1, which corresponds to N = 6 (red line, Figure 5D). Changing the value of L changes the length d_m (Figure 5F) and thus alters the N value at which this transition occurs (black lines, Figure 5D). The long-axis orientation of *M* is thus determined by the interplay between the polygon class and apposed side length of each neighbor, *N*. In the *Drosophila* wing disc, the value of L fluctuates by about 40% on average (Table 1). Equation (2) predicts that a 40% deviation in L value would change the point of rotation by only a single N value, suggesting that cleavage-plane bias should be noisy yet reproducible.

Supporting this analysis, cell size has a surprisingly weak influence compared to polygon class in our mechanical simulations (Figure S4). Consistent with our simulations, based on live-imaging analysis of local neighborhoods surrounding dividing cells in the *Drosophila* wing disc epithelium, there was no discernable difference in average area for cells occupying the cleavage-plane position (Figure S4D). We conclude that

Table 1. The Effective L Value Changes by Approximately 40% in Wild-Type *Drosophila* Tissues

N Cell Polygon Class	Average Effective L Value	Standard Deviation in Effective L Value	Sample Size(Hexagonal Interfaces with N Cells)
4	1.2504	.4165	22 interfaces
5	1.1158	.4141	231 interfaces
6	1.0580	.4053	487 interfaces
7	.9237	.4081	341 interfaces
8	.9620	.5405	46 interfaces

For each value of N (column 1), the average effective L value has been computed (column 2), as well as the sample standard deviation (column 3), using empirically extracted cellular networks from the *Drosophila* wing imaginal disc (Extended Experimental Procedures). The sample size for each calculation is given in column 4. The effective L value, computed for hexagonal cells, is the average value of an edge shared with an N-sided neighbor, divided by the average length of the remaining 5 edges.

internal angle constraints linked to the polygon class of neighboring cells are likely the dominant cause of cleavage-plane bias, with a lesser contribution from the effects of differential side lengths.

Cleavage-Plane Bias Is Predicted to Alter Global Tissue Topology

Numerous recent studies have used mathematical or computational approaches to understand the equilibrium topology of proliferating epithelia (Aegerter-Wilmsen et al., 2010; Cowan and Morris, 1988; Dubertret et al., 1998; Dubertret and Rivier, 1997; Gibson et al., 2006; Korn and Spalding, 1973; Miri and Rivier, 2006; Patel et al., 2009). Intuitively, cleavage-plane bias must alter the topology of a cell sheet because it modulates the rates at which specific polygon classes gain sides due to neighbor cell mitoses. We therefore investigated the implications of cleavage-plane bias for the distribution of polygonal cell shapes. We used two distinct computational simulations informed by the empirical division parameters (Figures S2A–S2C) to model global topology with and without cleavage-plane bias (Figure 6, Figure S5, and Figure S6). For both simulation types, the cleavage-plane bias values approximated those measured empirically (Figure S5F and Figure S6H). Both an abstract, topological simulator using a Monte-Carlo framework based on topological weights (Figure 6A) (Patel et al., 2009) and a mechanical model of tissue growth based on long-axis divisions (Figure 6D) (Brodland and Veldhuis, 2002) confirmed that cleavage-plane bias affects the frequency of hexagonal cells (Figures 6B and 6E). Moreover, the distribution of mitotic polygonal cells was severely disrupted in the absence of bias, resulting in decreased frequencies of heptagons and increased frequencies of octagons and nonagons (Figures 6C and 6F). Taken together, these results suggest that cleavage-plane bias is required to achieve the normal equilibrium distribution of cell shapes.

DISCUSSION

The results presented here raise several important questions. First, although our analysis provides a geometrical rationale for cleavage-plane bias based on interphase polygon topology (Figure 5), we still cannot rule out the simultaneous action of molecular cues at the cell cortex. In metazoans, epithelial cells often undergo mitosis-induced deformation prior to cleavage (Figures 3C and 3C′; Figures 4A and 4A′) (Gibson et al., 2006; Théry and Bornens, 2008), and our live-imaging results from *Drosophila* strongly suggest that a cellular long axis present in interphase can inform spindle orientation during mitosis (Figure 4). One intriguing possibility is that the interphase distribution of cell-cell contacts determines the localization of cortical cues important for spindle alignment, as has been previously reported (Théry et al., 2005, 2007).

For plant cells, by contrast, our results indicate that local cell packing influences, either directly or indirectly, the placement of the phragmosome and/or pre-prophase band (Pickett-Heaps and Northcote, 1966; Sinnott and Bloch, 1940). There are multiple ways in which this might be accomplished, potentially including stress- or strain-sensing mechanisms (Hamant et al., 2008; Lintilhac and Vesecky, 1984; Lynch and Lintilhac, 1997) or, more simply, based on cytoskeletal mechanisms that are able to sense cell shape (Flanders et al., 1990; Goodbody et al., 1991; Katsuta et al., 1990). To conclude, in addition to our purely geometrical interpretation, our results are also consistent with a hypothesis that both in animals and in plants, local epithelial topology may coordinately specify both the cellular long axis and the distribution of cortical determinants of the eventual cleavage plane.

A second important question concerns the broader implications of cleavage-plane bias for the emergence of cell shape. Previous studies of proliferating cell sheets in *Drosophila* and in *Cucumis* have shown that the distribution of mitotic cell shapes is shifted to have a heptagonal mean, as opposed to the hexagonal mean observed in the population of cells overall (Aegerter-Wilmsen et al., 2010; Gibson et al., 2006; Lewis, 1928). Our simulations (Figures 6A and 6D) suggest that the mitotic cell distribution is disrupted in the absence of cleavage-plane bias (Figures 6C and 6F), which is consistent with the view that in both *Drosophila* and *Cucumis*, interphase cells passively gain additional sides as a consequence of neighbor cell divisions. This interpretation contrasts with the idea that the mitotic shift solely reflects modulation of the cell cycle by topology-dependent mechanical stress (Aegerter-Wilmsen et al., 2010). Moreover, cleavage-plane bias is actually expected to synergize with the mitotic shift. By enriching for superhexagonal cells in the mitotic cell population, which are entropically favored to neighbor subhexagonal cells (Peshkin et al., 1991), the mitotic shift intuitively must amplify the effects of cleavage-plane bias.

In summary, by varying the orientation of cell division based on neighbor cell geometry, cells and tissues are able to achieve increased geometric regularity via a dynamic, topology-mediated feedback and control system. Precisely how the default geometric forces that bias cleavage-plane orientation interact with other mechanisms of division-plane control (Baena-López et al., 2005; Gong et al., 2004; Li et al., 2009; Ségalen et al., 2010; Siller et al., 2006; Willemsen et al., 2008) should be an important avenue for future research.

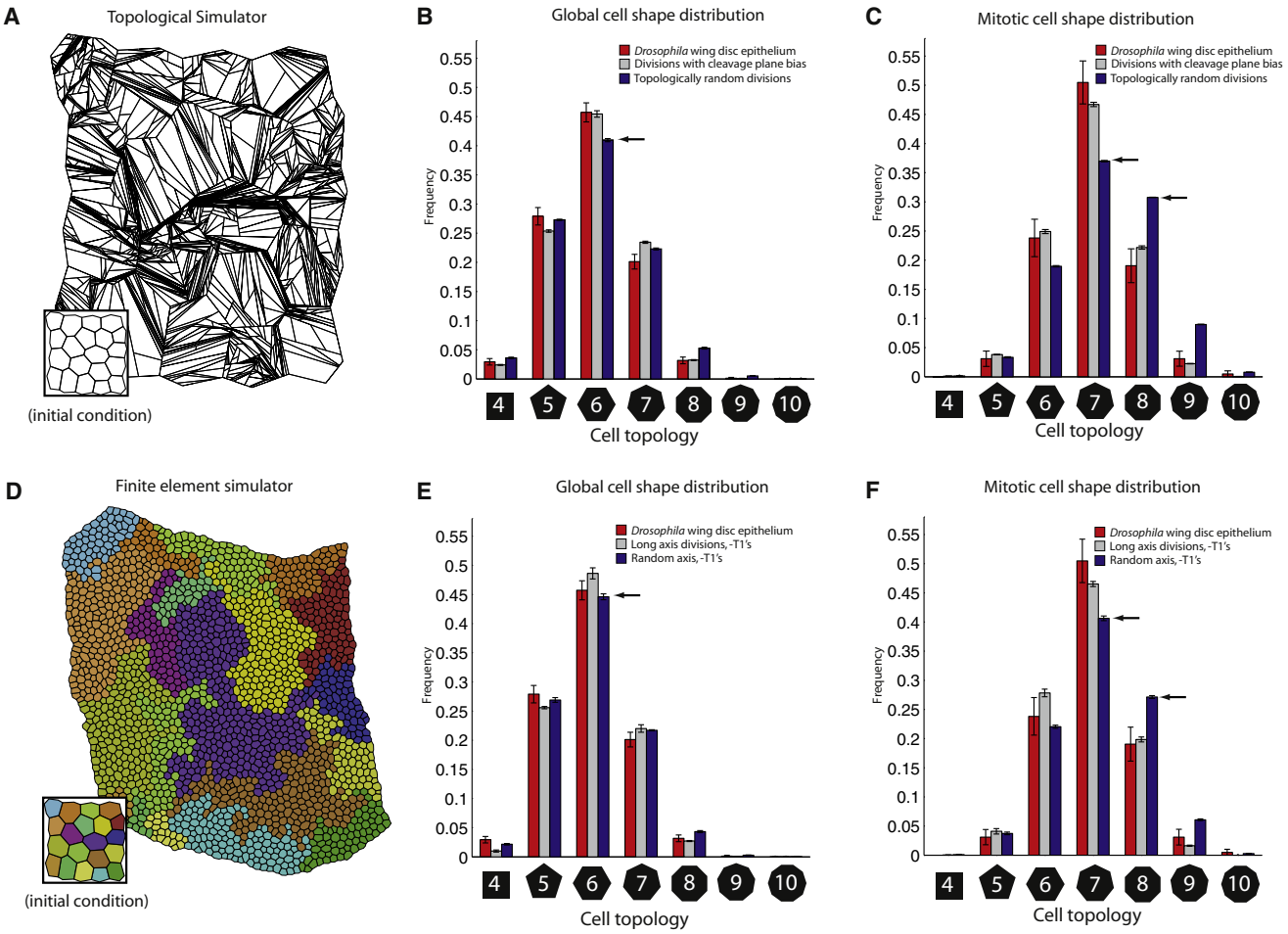

Figure 6. Cleavage-Plane Bias Participates in Cell Shape Emergence and Is Required for Normal Cell Packing

(A) The topological simulator does not model cellular mechanics but does explicitly keep track of topological neighbor relationships. Based on topological weights, the division likelihood, division symmetry, and cleavage-plane bias are approximately matched to empirically measured statistics in a Monte-Carlo framework (see Figures S2A–S2C).

(B) Hexagonal frequency declines by approximately 4% in the absence of bias. Arrows highlight this difference.

(C) The distribution of mitotic cells shows pronounced alterations in the absence of bias. Arrows highlight the differences.

(D) The finite element simulator models cellular mechanics, division, and rearrangement. The simulator captures mechanics in terms of a net, interfacial tension, which is modeled using rod-like finite elements. Division likelihoods are informed by the empirically measured values (Figure S2A). Cleavage-plane bias approximates the empirical values and is achieved using long-axis divisions. For finite element simulations incorporating cellular rearrangements (T1 transitions), see Figure S6.

(E) In the absence of bias, hexagonal frequency declines by about 4% (compare with panel B).

(F) The distribution of mitotic cells again shows pronounced alterations (compare with panel C).

Error bars in (B), (C), (E), and (F) represent ±1 SD. See also Figure S5 and Figure S6.

EXPERIMENTAL PROCEDURES

Fly Strains

To visualize the septate junctions, we used a *neuroglian-gfp* exon trap line, which was described in a previous study (*nrg-gfp*; Morin et al., 2001). To visualize the chromosomes in parallel, we generated a stock also carrying a Histone-H2 RFP marker (Schuh et al., 2007; Bloomington stock 23650).

Wing Disc Sample Preparation and Imaging

Wing discs were dissected from wandering 3rd instar larvae in Ringers' solution, fixed in 4% paraformaldehyde in PBS, and mounted in 70% glycerol/PBS. For live imaging, discs were carefully dissected and placed in a 50:50 mixture of Ringer's solution (130 mM NaCl, 5 mM KCl, 1.5 mM $MgCl_2$) and a second solution (adapted from Aldaz et al., 2010), consisting of 2% FBS (GIBCO) and 0.5% Pen/Strep (GIBCO; 5000 units/ml penicillin; 5000 μg/ml streptomycin) in Shields and Sang M3 Insect media (Sigma). Live discs were mounted between two pieces of Scotch double-sided tape (3M). Air bubbles were added to the medium using an insulin syringe (BD Ultra-fine with a 30-gauge needle) to potentiate gas exchange. Wing discs were maintained in culture for up to 4 hr and imaged at intervals of 15–30 s. All samples, live and fixed, were imaged on a Leica SP5 or Leica SP2 confocal microscope with a 63× glycerol or oil objective.

Cucumis Sample Preparation and Imaging

Epidermis was collected from freshly gathered cucumbers approximately 10 cm in length and 2 cm in diameter (Red Ridge Farm, Odessa, MO, USA).

Epidermis was peeled in thin layers and fixed in 4% paraformaldehyde in 50 mM KPO_4, 5.0 mM EDTA, and 0.2% Tween20 (pH 7) for at least 2 hr at room temperature (adapted from Gallagher and Smith, 1999). Tissue pieces were then washed 2–5 times in dH_2O and incubated in 5 mg/ml Calcofluor White (Sigma) in PBS for at least 10 min before imaging. Images were collected using a Zeiss LSM 510 Meta with a 20× Plan-Apochromat objective, NA 0.8.

Error Bars

Unless otherwise specified, error bars refer to a single standard deviation. For the case of ratio distributions, we have reported an average value of the standard deviation. This was computed as follows: the data were randomized and broken into three subsamples of equal size in order to compute an average value for the standard deviation, based on 1000 random shuffles of the data.

Annotation of *Drosophila* Wing Disc Cytokinetic Figures in Fixed Preparations

A total of 420 cytokinetic figures and their 2946 cellular neighbors were scored by hand, in multiple focal planes to ensure accuracy of topological counts. Out of the 2946 neighbors, 840, or exactly two per cytokinetic figure, were designated as being in the division-plane position. Cells were interpreted to be in the division-plane position when they occupied the majority of the cytokinetic furrow. Due to the ambiguity of division ordering, cytokinetic figures adjacent to other cytokinetic figures were not considered for analysis.

Annotation of Fixed *Drosophila* Wing Disc Epithelial Cell Sheets

Images of contiguous epithelial regions from *Drosophila* wing disc epithelia were annotated by hand using Microsoft Powerpoint. We used custom-built software to digitize the annotations for analysis in MATLAB. A total of three such cell sheets, containing 254, 195, and 233 cells, respectively, were analyzed to compute the effective L value (Figure 5C; Table 1), which is described in the text. See the Extended Experimental Procedures for additional details.

Live-Imaging Analysis of Mitosis in the *Drosophila* Wing Disc

From live movies, a total of 198 mitotic cells in the *Drosophila* wing disc epithelium were analyzed by hand using ImageJ. With the exception of cells located on compartment boundaries, every scoreable cell on the epithelium was used. To control for possible mechanical influences due to neighboring divisions, we did not consider dividing cells neighboring each other to be scoreable if they rounded up at the same time. Interphase geometry measurements were based on the earliest available time point (the first movie frame), except in rare cases when epithelial morphology obscured the cell in question, in which case a slightly later time point was used. The long-axis orientation of each cell was computed using ImageJ, including curvature, based on manual input from the Polygon Selections tool. The identical procedure was used for each cell at later stages, including the eventual cytokinetic figure (see Figure 4A′ for an illustration). See the Extended Experimental Procedures for additional details.

Analysis of *Cucumis* Epidermal Cell Sheets

Images of contiguous regions of *Cucumis* epidermis were annotated by hand using ImageJ. Cell geometry was outlined using the Polygon Selections tool, with one node placed per tri-cellular junction, except in cases of very curved cellular edges, in which additional nodes were used to increase annotation accuracy. To visualize the ellipse of best fit to cell geometry, we used a custom-made ImageJ macro. See the Extended Experimental Procedures for additional information.

Algorithm for Computing the Minimal Energy Configuration for Local Cellular Neighborhoods

We used a mechanical relaxation algorithm for cellular networks that has been previously described (Prusinkiewicz and Lindenmayer, 1990). For relaxation (Figure 1), cellular networks were modeled in terms of a balance between edge length tensions (described using ideal springs) and internal pressure (Figure S1). Relaxation was implemented in terms of a system of ordinary differential equations that were solved numerically using the ODE45 solver in MATLAB (Mathworks). See the Extended Experimental Procedures for additional information.

Topological Simulations of Proliferation

Proliferation was simulated in terms of a network containing exclusively tricellular nodes, with wrapping boundary conditions. All division parameters, including division likelihoods of polygonal cells, the statistical partitioning of mother cell nodes, and the likelihoods of orienting the division plane in the direction of specific polygonal neighbor cell types, are matched to the empirically measured statistics for the *Drosophila* wing disc (see Figures S2A–S2C). The algorithmic details are described in the Extended Experimental Procedures.

Finite Element Models of Proliferating Cell Sheets

The FEM simulations (Brodland and Veldhuis, 2002; Chen and Brodland, 2000) model apical contractility, cell-cell adhesion, and all other forces along the cellular edge lengths in terms of a net, interfacial tension, γ, which is generated by rod-like finite elements. Proliferation is modeled in terms of long-axis divisions. Cell-cell rearrangements (T1 transitions) are permitted when cellular edge lengths shrink below a threshold value. See Figure S6 for a comparison between simulations in which T1 transitions are active, versus those for which they are inactive. Additional details are described in the Extended Experimental Procedures.

SUPPLEMENTAL INFORMATION

Supplemental Information includes Extended Experimental Procedures, six figures, and one movie and can be found with this article online at doi:10.1016/j.cell.2010.12.035.

ACKNOWLEDGMENTS

The authors gratefully acknowledge support for this research from the Stowers Institute for Medical Research and the Burroughs Wellcome Fund (to M.C.G.), from the National Science Foundation (to R.N.), from the Natural Sciences and Engineering Research Council of Canada (to G.W.B.), and from the Howard Hughes Medical Institute (to N.P.). W.T.G. was supported in part by NIH/NIGMS Molecular Biophysics Training Grant #T32 GM008313 and CTC grant 1029 to M.C.G.

Received: June 22, 2010
Revised: November 4, 2010
Accepted: December 15, 2010
Published: February 3, 2011

REFERENCES

Aegerter-Wilmsen, T., Smith, A.C., Christen, A.J., Aegerter, C.M., Hafen, E., and Basler, K. (2010). Exploring the effects of mechanical feedback on epithelial topology. Development *137*, 499–506.

Aldaz, S., Escudero, L.M., and Freeman, M. (2010). Live imaging of Drosophila imaginal disc development. Proc. Natl. Acad. Sci. USA *107*, 14217–14222.

Baena-López, L.A., Baonza, A., and García-Bellido, A. (2005). The orientation of cell divisions determines the shape of *Drosophila* organs. Curr. Biol. *15*, 1640–1644.

Black, S.D., and Vincent, J.P. (1988). The first cleavage plane and the embryonic axis are determined by separate mechanisms in Xenopus laevis. II. Experimental dissociation by lateral compression of the egg. Dev. Biol. *128*, 65–71.

Brodland, G.W., and Veldhuis, J.H. (2002). Computer simulations of mitosis and interdependencies between mitosis orientation, cell shape and epithelia reshaping. J. Biomech. *35*, 673–681.

Buschmann, H., Chan, J., Sanchez-Pulido, L., Andrade-Navarro, M.A., Doonan, J.H., and Lloyd, C.W. (2006). Microtubule-associated AIR9 recognizes the cortical division site at preprophase and cell-plate insertion. Curr. Biol. *16*, 1938–1943.

Chen, H.H., and Brodland, G.W. (2000). Cell-level finite element studies of viscous cells in planar aggregates. J. Biomech. Eng. *122*, 394–401.

Cowan, R., and Morris, V.B. (1988). Division rules for polygonal cells. J. Theor. Biol. *131*, 33–42.

Dubertret, B., and Rivier, N. (1997). The renewal of the epidermis: A topological mechanism. Biophys. J. *73*, 38–44.

Dubertret, B., Aste, T., Ohlenbusch, H.M., and Rivier, N. (1998). Two-dimensional froths and the dynamics of biological tissues. Phys. Rev. E Stat. Phys. Plasmas Fluids Relat. Interdiscip. Topics *58*, 6368–6378.

Fernández-Miñán, A., Martín-Bermudo, M.D., and González-Reyes, A. (2007). Integrin signaling regulates spindle orientation in *Drosophila* to preserve the follicular-epithelium monolayer. Curr. Biol. *17*, 683–688.

Fischer, E., Legue, E., Doyen, A., Nato, F., Nicolas, J.F., Torres, V., Yaniv, M., and Pontoglio, M. (2006). Defective planar cell polarity in polycystic kidney disease. Nat. Genet. *38*, 21–23.

Flanders, D.J., Rawlins, D.J., Shaw, P.J., and Lloyd, C.W. (1990). Nucleus-associated microtubules help determine the division plane of plant epidermal cells: avoidance of four-way junctions and the role of cell geometry. J. Cell Biol. *110*, 1111–1122.

Gallagher, K., and Smith, L.G. (1999). discordia mutations specifically misorient asymmetric cell divisions during development of the maize leaf epidermis. Development *126*, 4623–4633.

Gibson, M.C., Patel, A.B., Nagpal, R., and Perrimon, N. (2006). The emergence of geometric order in proliferating metazoan epithelia. Nature *442*, 1038–1041.

Gong, Y., Mo, C., and Fraser, S.E. (2004). Planar cell polarity signalling controls cell division orientation during zebrafish gastrulation. Nature *430*, 689–693.

Goodbody, K.C., Venverloo, C.J., and Lloyd, C.W. (1991). Laser microsurgery demonstrates that cytoplasmic strands anchoring the nucleus across the vacuole of premitotic plant cells are under tension. Implications for division plane alignment. Development *113*, 931–939.

Gray, D., Plusa, B., Piotrowska, K., Na, J., Tom, B., Glover, D.M., and Zernicka-Goetz, M. (2004). First cleavage of the mouse embryo responds to change in egg shape at fertilization. Curr. Biol. *14*, 397–405.

Hamant, O., Heisler, M.G., Jönsson, H., Krupinski, P., Uyttewaal, M., Bokov, P., Corson, F., Sahlin, P., Boudaoud, A., Meyerowitz, E.M., et al. (2008). Developmental patterning by mechanical signals in Arabidopsis. Science *322*, 1650–1655.

Hofmeister, W. (1863). Zusatze und Berichtigungen zu den 1851 veröffentlichen Untersuchungengen der Entwicklung höherer Kryptogamen. Jahrbucher für Wissenschaft und Botanik *3*, 259–293.

Johnston, C.A., Hirono, K., Prehoda, K.E., and Doe, C.Q. (2009). Identification of an Aurora-A/PinsLINKER/Dlg spindle orientation pathway using induced cell polarity in S2 cells. Cell *138*, 1150–1163.

Katsuta, J., Hashiguchi, Y., and Shibaoka, H. (1990). The role of the cytoskeleton in positioning of the nucleus in premitotic tobacco by-2 cells. J. Cell Sci. *95*, 413–422.

Korn, R.W., and Spalding, R.M. (1973). The geometry of plant epidermal cells. New Phytol. *72*, 1357–1365.

Kost, B., and Chua, N.H. (2002). The plant cytoskeleton: Vacuoles and cell walls make the difference. Cell *108*, 9–12.

Lewis, F.T. (1928). The correlation between cell division and the shapes and sizes of prismatic cells in the epidermis of cucumis. Anat. Rec. *38*, 341–376.

Li, W., Kale, A., and Baker, N.E. (2009). Oriented cell division as a response to cell death and cell competition. Curr. Biol. *19*, 1821–1826.

Lintilhac, P.M., and Vesecky, T.B. (1984). Stress-induced alignment of division plane in plant tissues grown *in vitro*. Nature *307*, 363–364.

Lloyd, C.W. (1991). How does the cytoskeleton read the laws of geometry in aligning the division plane of plant-cells. Development Suppl. *1*, 55–65.

Lynch, T.M., and Lintilhac, P.M. (1997). Mechanical signals in plant development: a new method for single cell studies. Dev. Biol. *181*, 246–256.

Miri, M., and Rivier, N. (2006). Universality in two-dimensional cellular structures evolving by cell division and disappearance. Phys. Rev. E Stat. Nonlin. Soft Matter Phys. *73*, 031101.

Morin, X., Daneman, R., Zavortink, M., and Chia, W. (2001). A protein trap strategy to detect GFP-tagged proteins expressed from their endogenous loci in Drosophila. Proc. Natl. Acad. Sci. USA *98*, 15050–15055.

O'Connell, C.B., and Wang, Y.L. (2000). Mammalian spindle orientation and position respond to changes in cell shape in a dynein-dependent fashion. Mol. Biol. Cell *11*, 1765–1774.

Palevitz, B.A. (1987). Actin in the preprophase band of Allium cepa. J. Cell Biol. *104*, 1515–1519.

Patel, A.B., Gibson, W.T., Gibson, M.C., and Nagpal, R. (2009). Modeling and inferring cleavage patterns in proliferating epithelia. PLoS Comput. Biol. *5*, e1000412.

Peshkin, M.A., Strandburg, K.J., and Rivier, N. (1991). Entropic predictions for cellular networks. Phys. Rev. Lett. *67*, 1803–1806.

Pickett-Heaps, J.D., and Northcote, D.H. (1966). Organization of microtubules and endoplasmic reticulum during mitosis and cytokinesis in wheat meristems. J. Cell Sci. *1*, 109–120.

Prusinkiewicz, P., and Lindenmayer, A. (1990). The Algorithmic Beauty of Plants (New York: Springer-Verlag).

Quyn, A.J., Appleton, P.L., Carey, F.A., Steele, R.J., Barker, N., Clevers, H., Ridgway, R.A., Sansom, O.J., and Näthke, I.S. (2010). Spindle orientation bias in gut epithelial stem cell compartments is lost in precancerous tissue. Cell Stem Cell *6*, 175–181.

Rivier, N., and Lissowski, A. (1982). On the correlation between sizes and shapes of cells in epithelial mosaics. J. Phys. Math. Gen. *15*, L143–L148.

Rivier, N., Schliecker, G., and Dubertret, B. (1995). The stationary state of epithelia. Acta Biotheor. *43*, 403–423.

Saburi, S., Hester, I., Fischer, E., Pontoglio, M., Eremina, V., Gessler, M., Quaggin, S.E., Harrison, R., Mount, R., and McNeill, H. (2008). Loss of Fat4 disrupts PCP signaling and oriented cell division and leads to cystic kidney disease. Nat. Genet. *40*, 1010–1015.

Schuh, M., Lehner, C.F., and Heidmann, S. (2007). Incorporation of *Drosophila* CID/CENP-A and CENP-C into centromeres during early embryonic anaphase. Curr. Biol. *17*, 237–243.

Ségalen, M., Johnston, C.A., Martin, C.A., Dumortier, J.G., Prehoda, K.E., David, N.B., Doe, C.Q., and Bellaïche, Y. (2010). The Fz-Dsh planar cell polarity pathway induces oriented cell division via Mud/NuMA in *Drosophila* and zebrafish. Dev. Cell *19*, 740–752.

Siller, K.H., and Doe, C.Q. (2009). Spindle orientation during asymmetric cell division. Nat. Cell Biol. *11*, 365–374.

Siller, K.H., Cabernard, C., and Doe, C.Q. (2006). The NuMA-related Mud protein binds Pins and regulates spindle orientation in Drosophila neuroblasts. Nat. Cell Biol. *8*, 594–600.

Sinnott, E.W., and Bloch, R. (1940). Cytoplasmic behavior during division of vacuolate plant cells. Proc. Natl. Acad. Sci. USA *26*, 223–227.

Speicher, S., Fischer, A., Knoblich, J., and Carmena, A. (2008). The PDZ protein Canoe regulates the asymmetric division of *Drosophila* neuroblasts and muscle progenitors. Curr. Biol. *18*, 831–837.

Strauss, B., Adams, R.J., and Papalopulu, N. (2006). A default mechanism of spindle orientation based on cell shape is sufficient to generate cell fate diversity in polarised Xenopus blastomeres. Development *133*, 3883–3893.

Théry, M., and Bornens, M. (2008). Get round and stiff for mitosis. HFSP J *2*, 65–71.

Théry, M., Jiménez-Dalmaroni, A., Racine, V., Bornens, M., and Jülicher, F. (2007). Experimental and theoretical study of mitotic spindle orientation. Nature *447*, 493–496.

Théry, M., Racine, V., Pépin, A., Piel, M., Chen, Y., Sibarita, J.B., and Bornens, M. (2005). The extracellular matrix guides the orientation of the cell division axis. Nat. Cell Biol. *7*, 947–953.

Traas, J., Bellini, C., Nacry, P., Kronenberger, J., Bouchez, D., and Caboche, M. (1995). Normal differentiation patterns in plants lacking microtubular preprophase bands. Nature *375*, 676–677.

Vanstraelen, M., Van Damme, D., De Rycke, R., Mylle, E., Inzé, D., and Geelen, D. (2006). Cell cycle-dependent targeting of a kinesin at the plasma membrane demarcates the division site in plant cells. Curr. Biol. *16*, 308–314.

Walker, K.L., Müller, S., Moss, D., Ehrhardt, D.W., and Smith, L.G. (2007). Arabidopsis TANGLED identifies the division plane throughout mitosis and cytokinesis. Curr. Biol. *17*, 1827–1836.

Willemsen, V., Bauch, M., Bennett, T., Campilho, A., Wolkenfelt, H., Xu, J., Haseloff, J., and Scheres, B. (2008). The NAC domain transcription factors FEZ and SOMBRERO control the orientation of cell division plane in *Arabidopsis* root stem cells. Dev. Cell *15*, 913–922.

Wright, A.J., Gallagher, K., and Smith, L.G. (2009). discordia1 and alternative discordia1 function redundantly at the cortical division site to promote preprophase band formation and orient division planes in maize. Plant Cell *21*, 234–247.